Engineering Structures 213 (2020) 110592

Contents lists available at ScienceDirect

Engineering Structures

journal homepage: www.elsevier.com/locate/engstruct

Stress-laminated timber decks in bridges: Friction between lamellas, butt joints and pre-stressing system

Francesco Mirko Massaro*, Kjell Arne Malo

Department of Structural Engineering, Norwegian University of Science and Technology (NTNU), Rich. Birkelandsvei 1A, 7491 Trondheim, Norway

ARTICLE INFO

Keywords:
Stress-laminated timber decks
Timber bridges
Butt joints
Stiffness
Friction
Pre-stress

ABSTRACT

Stress-laminated timber (SLT) decks in bridges are popular structural systems in bridge engineering. SLT decks are made from parallel timber beams placed side by side and pre-stressed together by means of steel rods. SLT decks can be in any length by just using displaced butt joints. The paper presents results from friction experiments performed in both grain and transverse direction with different levels of pre-stress. Numerical simulations of these experiments in addition to comparisons to full-scale experiments of SLT decks presented in literature verified the numerical model approach. Furthermore, several alternative SLT deck configurations with different amounts of butt joints and pre-stressing rod locations were modelled to study their influence on the structural properties of SLT decks. Finally, some recommendations on design of SLT bridge decks are given.

1. Introduction

Stress-laminated timber (SLT) bridge decks were developed in North America in the late nineteen-seventies. In the subsequent decades, this deck concept started to be utilized also elsewhere, especially in Australia and in the Nordic European countries [1]. SLT decks consist of parallel timber beams stacked side by side, most commonly with their longitudinal direction parallel to the long direction of the deck. The beams (lamellas) are mechanically held together by pre-stressed (steel) rods, installed in pre-drilled holes in the perpendicular direction relative to the grain and lamella axes. The pre-stressing rods are most frequently positioned in the central part of the lamella, as shown in the SLT deck in Fig. 1. However, different rods arrangements are also employed in recent constructions where e.g. two rows of pre-stressing rods are used (see Fig. 2).

The pre-stressing force must be sufficiently high in order to avert gaps between the lamellas as well as vertical slips between the lamellas (Fig. 3a-b). Gaps are prevented by the distribution of the compressive stresses, whereas slips are avoided due to the frictional forces between the lamellas generated by the pre-stress. Avoiding these mechanisms, SLT decks behave like an orthotropic plate [2,3].

However, the application of the pre-stress, e.g. through the systems displayed in Figs. 1b and 2b, may generate high local compression stress in the perpendicular direction to the grain under the anchor plates [4]. The pre-stressing force is not constant during the lifetime of the SLT deck but losses occur due to local deformations of timber, hygroscopic deformations and long-term effects of timber.

Each lamella usually consists of several beam elements, just placed in the longitudinal direction without any splicing in the length direction, with the end faces of adjacent laminations merely facing each other. The resulting possible gaps in the length direction are usually denoted as *butt joints*. The use of butt joints allows spans larger than the beams length. Indeed, SLT decks can nowadays be produced in almost any length or width. However, the butt joints cannot transfer bending moment, thus they are reducing the flexural stiffness of the deck. Therefore, in order to avoid weak sections, the butt joints are usually displaced across the deck. A typical disposition of the butt joints distribution is shown in Fig. 3c. The first guidelines about the design of SLT decks, published by Ritter and the US Forest Service [5], suggested that, within a distance of approximately 1.2 m, not more than one in four adjacent beams should be butt jointed [6,7]. The reduction of flexural stiffness is taken into account by several authors, and regulations based on the butt joint frequency, or on the number of beams per butt joint, in a transversal section of the SLT deck have been proposed [5,7–9]. Therefore, friction plays an important role regarding both the effect of butt joints and possible vertical slips between the timber beams [10] (Fig. 3b). A study by Kalbitzer on softwood addressed the influence of moisture content, surface roughness and sliding direction relative to the grain direction of timber, on the friction coefficient between mating timber surfaces [11].

The main objective of the present work is to study the behavior of SLT decks, exploring the influence of butt joints on the stiffness of this structural decking system. In order to achieve the objective, an experimental study together with numerical simulations of friction

* Corresponding author.
E-mail address: francesco.m.massaro@ntnu.no (F.M. Massaro).

https://doi.org/10.1016/j.engstruct.2020.110592
Received 4 October 2019; Received in revised form 14 February 2020; Accepted 29 March 2020

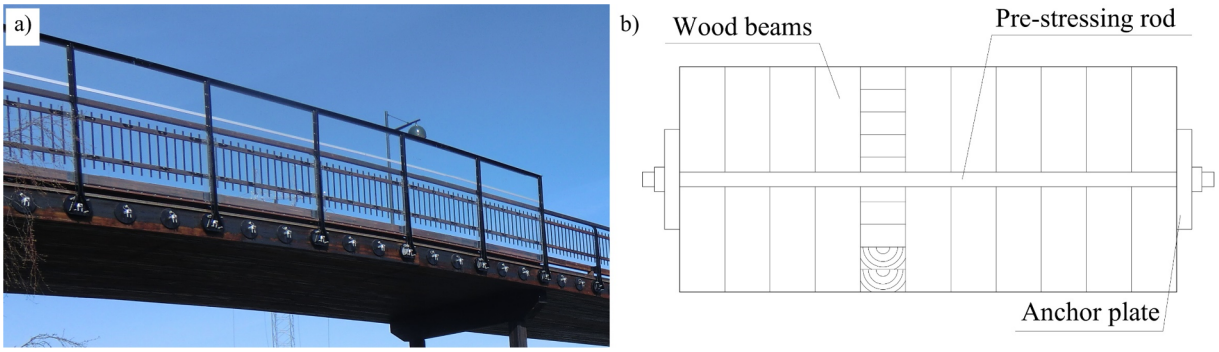

Fig. 1. a) SLT bridge deck - Ladebrua in Trondheim, Norway; b) Transversal cross-section of a SLT deck.

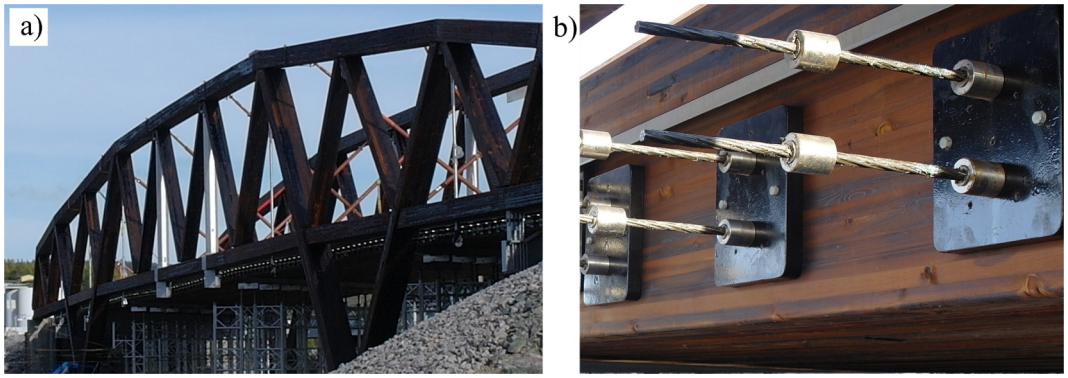

Fig. 2. a) Norsenga Bridge in Kongsvinger, Norway; b) Detail of the pre-stressing system.

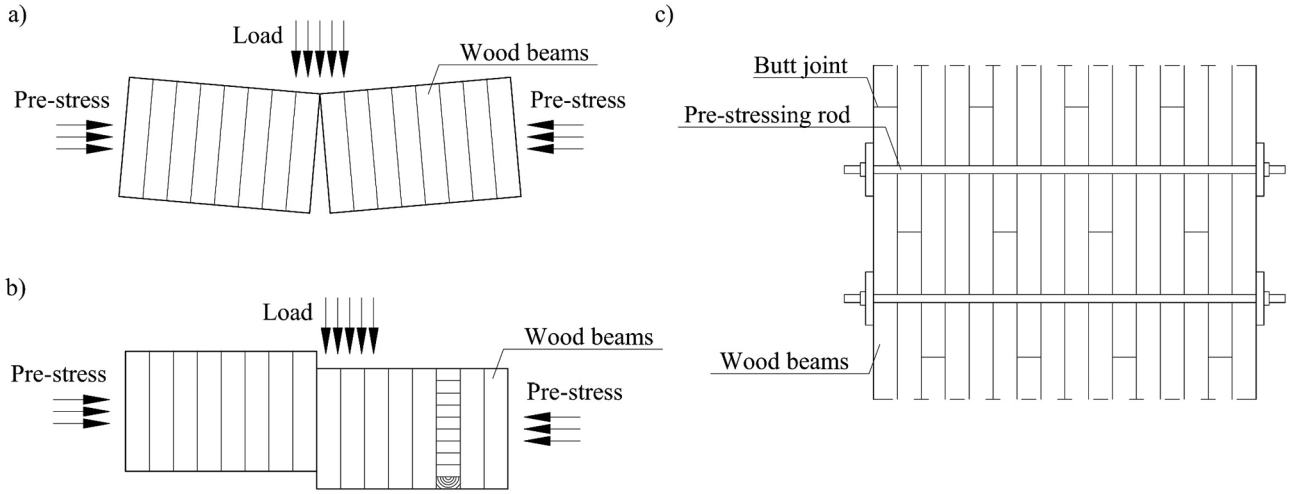

Fig. 3. a-b) Mechanisms to prevent in SLT decks: a) gap; b) slip. c) Distribution of butt joints in SLT deck: in any transversal cross-section it is present not more than one butt joint per four adjacent beams.

between timber elements was performed, thus obtaining friction parameters and vertical slip data between timber surfaces. Furthermore, Dahl [12] performed full-scale tests on SLT decks showing the influence of the pre-stress level on the overall deck behavior. Herein, these results are compared to numerical simulations of the decks tested by Dahl. Moreover, numerical simulations of different SLT deck configurations, obtained by varying the geometry of the deck and number and locations of the butt joints, have been performed and the results are presented herein. Finally, a study on several pre-stressing arrangements of SLT decks with various rod locations has been performed by means of numerical simulations. The investigation on the distribution of stresses of the different arrangements permits a better understanding in order to avoid gaps between laminations (Fig. 3a).

For ease of readability, the paper describes and discusses firstly the friction experiments and simulations, thereafter the SLT deck experiment together with simulations, and conclusively the study of the alternative deck configurations (butt-joints configurations, pre-stress patterns and transverse tensile stress investigation).

2. Friction

2.1. Material and methods

The study on friction behavior was carried out by testing different pre-stress levels in both sliding directions (longitudinal and transversal to the wood fibers). The experimental setup was also modelled in the

finite element method (FEM) software program Abaqus [13]. The same numerical approach was thereafter used to perform numerical simulations of full-scale tests on SLT decks performed by Dahl [12,14]. Using the same numerical approach, several other SLT deck configurations, varying geometry, amount of butt joints, and pre-stressing rods arrangement, were numerically explored.

2.1.1. Experiments

The friction tests were conducted on Scots Pine (Pinus sylvestris) specimens classified as GL30h according to NS-EN 14080:2013 [15]. The timber was not impregnated nor treated with any chemicals. Each specimen was composed of three timber blocks, each with dimension 166 × 166 × 90 mm^3, and had planed sliding surfaces. An oversized hole of 50 mm diameter was drilled in the center of the cross-section of the blocks for insertion of a pre-stressing rod with diameter 30 mm. The hole had to be oversized in order to allow for the relative sliding of the timber blocks during the friction tests.

The experiment consisted of three phases: the first phase was the assembly and pre-stressing phase, the second phase was the re-assembling and the third phase was the testing and friction measurement. The three phases were performed at 20 °C of temperature and 65% relative humidity (RH) of the air, resulting in approximately 12% moisture content.

In the first phase, three timber blocks were pre-stressed together using a 30 mm diameter steel rod, depicted as Rod 1 in Fig. 4a, and two steel plates of dimensions 300 × 300 × 20 mm^3 (see Fig. 4), until the required uniform compression stress was reached. The value of the compression stress was verified using a load cell (LC in Fig. 4) located between one of the outer steel plates and the nut of the pre-stressing system. Then, the distance between the steel plates was measured with calipers Afterwards, two steel rods of 20 mm diameter, depicted as Rod 2 and Rod 3 in Fig. 4a, were inserted in the holes of the steel plates, outside of the timber blocks. The two rods were tightened, observing a decrease in the force in the Rod 1, until it was completely relaxed. Subsequently, the distance between the steel plates was again measured so as to verify that the distance between the two pre-stressing plates remained constant. Finally, Rod 1 was removed and the pre-stress was maintained by Rod 2 and Rod 3. The pre-stress was kept for a period of one week. This procedure was necessary in order to use the same load cell to prepare all the specimens and proceed with a sequence of parallel tests. Indeed, this procedure was repeated in the preparation of all the specimens. After the completion of the pre-stressing week, the second phase (re-assembling) started mounting again Rod 1 together with the load cell. The Rod 1 was tightened, while the load cell was measuring the force in the rod, until Rod 2 and Rod 3 were fully relaxed and thus removed, still maintaining constant the distance between the pre-stressing plates.

In the third phase, the friction tests were performed in a 100kN Instron universal test machine. The two external timber blocks were placed over two steel supports and the middle block was pushed by a steel loading block, in order to have a pressure as uniform as possible on the timber element (see Fig. 4b). The test was conducted in displacement control with a speed of 5 mm/min. In some of the experiments (the experiments 03 to 10 of the series T06 and the whole series L03, L06 and T03; see Table 1), an unloading and reloading cycle was performed about 140 s after the test start. This was done in order to see if the friction coefficient was changed due to an unloading and reloading cycle.

Two different configurations were tested: one with the timber fibers orientated collinearly with the external force direction (i.e. friction measurements in the longitudinal direction of the wood fibers; see

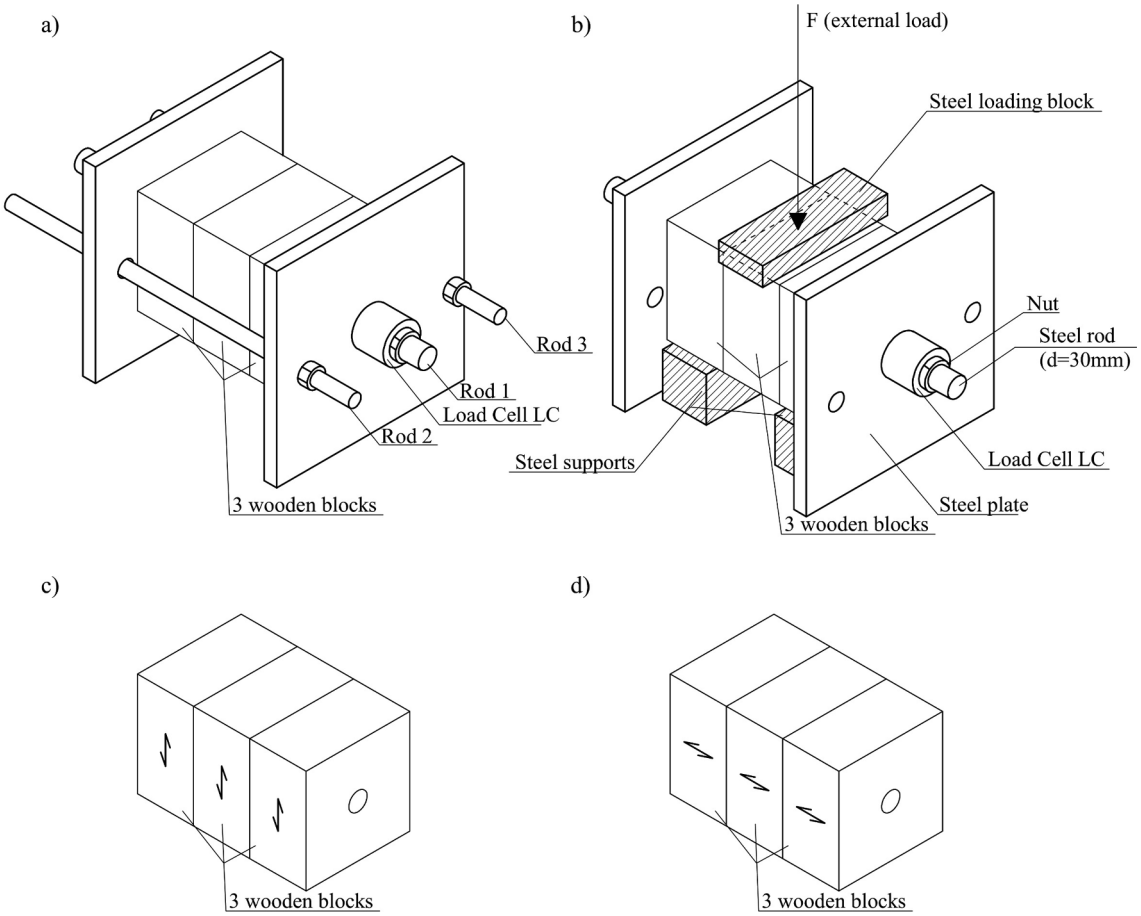

Fig. 4. Sketch of a specimen. a) During the pre-stress phase; b) During the friction test; c) Timber fibers orientation in Lxx series; d) Timber fibers orientation in Txx series.

Table 1
Summary of the performed experiments.

Series name	n. of tests	Sliding direction with respect to the wood fibers	Pre-stress [MPa]
T10	20	Transversal	1.0
L10	20	Longitudinal	1.0
T06	10	Transversal	0.6
L06	10	Longitudinal	0.6
T03	10	Transversal	0.3
L03	10	Longitudinal	0.3
T01	18	Transversal	0.1

Fig. 4c), and one with the timber fibers orientated orthogonally (i.e. friction measurements in the transversal direction of the wood fibers; see Fig. 4d). The experiments are denoted as shown in Table 1, where the Latin capital letter identifies the sliding direction with respect to fibers direction (T: transversal; L: longitudinal), followed by the indication of the pre-stressing load (the numbers 10, 06, 03 and 01 indicate an initial pre-stress of 1.0, 0.6, 0.3 and 0.1 MPa respectively).

2.1.2. Numerical simulations

The experimental setups were also modelled in the FEM software program Abaqus [13]. The geometry of the model resembled the experimental setups, but with exclusion of the rods (see Fig. 5).

Timber was modeled as an orthotropic material with coinciding properties in the two transversal directions. The transverse isotropy condition was however not fulfilled because the shear moduli are independent from the normal moduli. The nine material properties used in the numerical model were defined in a Cartesian coordinate system, and they are given in Table 2, where the subscript "0″ indicates the longitudinal direction, while the subscript "90" designates the two transversal ones. All Poisson's ratios were taken as zero. Eight-node solid brick elements (C3D8) were used in the model. Due to the double symmetry of the problem, only a quarter of the setup was modelled. The symmetry boundary conditions are displayed with the red diagonal cross pattern in Fig. 5. The contact between the timber blocks and between timber and steel elements was defined as "hard" contact for the normal behavior, while a penalty frictional formulation was used for the tangential behavior. The friction coefficient between steel and timber was chosen equal to 0.2 [16].

The analysis was carried in two subsequent steps: pre-stressing step and loading step. In the pre-stressing step, the pre-stressing plate moved along the positive x-axis in order to pre-compress the timber blocks with the required average stress value. In this step, the bottom surfaces of the two timber blocks and the pre-stressing steel plate were prevented to displace in the z-direction. In the following loading step, only the timber block A and the pre-stressing plate were prevented to move in the z-direction, while the timber block B was unsupported. Thus in this step, the loading steel plate moved in the negative z-direction up to 10 mm, and the timber block B was sliding on the block A.

Table 2
Elastic properties of wood used in numerical simulations (GL30h) [15].

Normal moduli	[MPa]	Shear moduli	[MPa]	Poisson's ratios	[–]
E_0	13,600	G_0	650	ν	0
E_{90}	300	G_{90}	65		

2.2. Results and discussion

2.2.1. Experiments

The results of the performed friction tests, described in Chapter 2.1.1, are given in Fig. 6. In each horizontal pair of graphs, the response is given by loading force vs. time, and pre-stressing force vs. time, for all specimens tested under the same pre-stress conditions. More results are given in Appendix A where each plot refers to the individual specimens.

The results to the left in Fig. 6 show initially a linear increase of the loading force corresponding to the static phase, followed by a drop in the force due to sliding, and thereafter a phase where the force remains fairly constant. This behavior is, to a certain extent, mirrored in the measured pre-stressing force (to the right in Fig. 6), especially in case of high pre-stressing force. In some of the specimens, the loading force increased again after the first drop, reaching a second peak, after which it decreased towards an asymptotic value. This effect might occur due to a slightly eccentric position of the load, or to dishomogeneities in the timber material and hence the transition from static and to kinetic friction is not concurrent for the entire contact surface.

The initial raising branch of the plots is used to evaluate the static friction, while the constant asymptotic branch after the peak is used for the evaluation of the kinetic friction. The static friction coefficient μ_{st} is evaluated by $\mu_{st} = F_{st}/2P_{st}$, where F_{st} is the force corresponding to the peak of the static branch, which generally is the maximum loading force applied from the machine, and P_{st} is the corresponding pre-stressing force at the same time. The kinetic friction coefficient μ_{ki} is evaluated

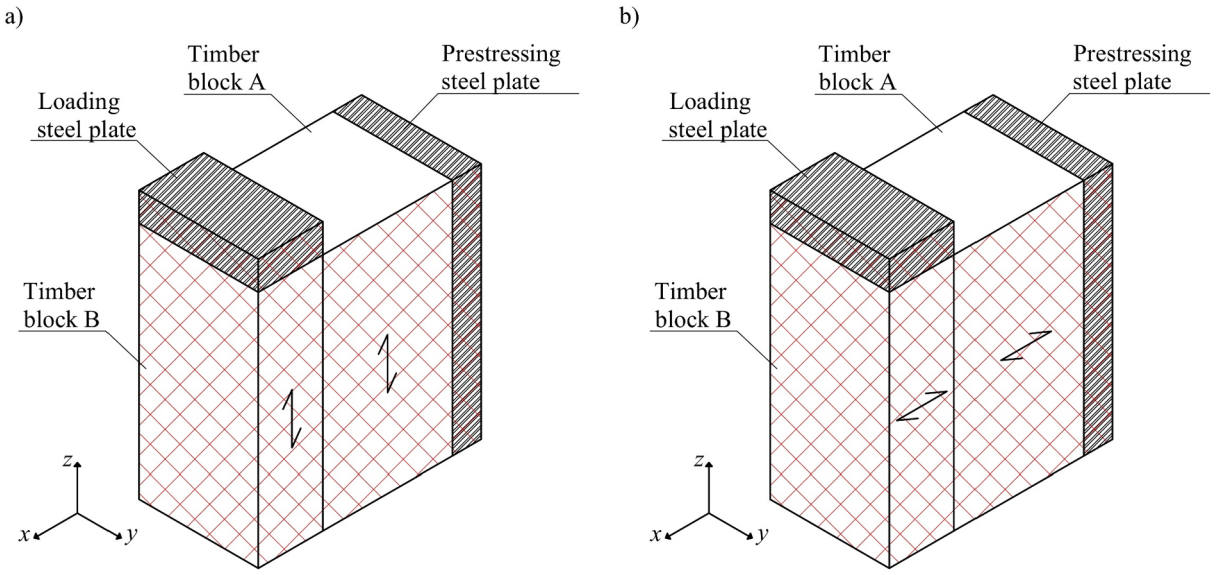

Fig. 5. Geometry of the numerical model of the friction experiment: a) Timber fibers orientation in Lxx series; b) Timber fibers orientation in Txx series.

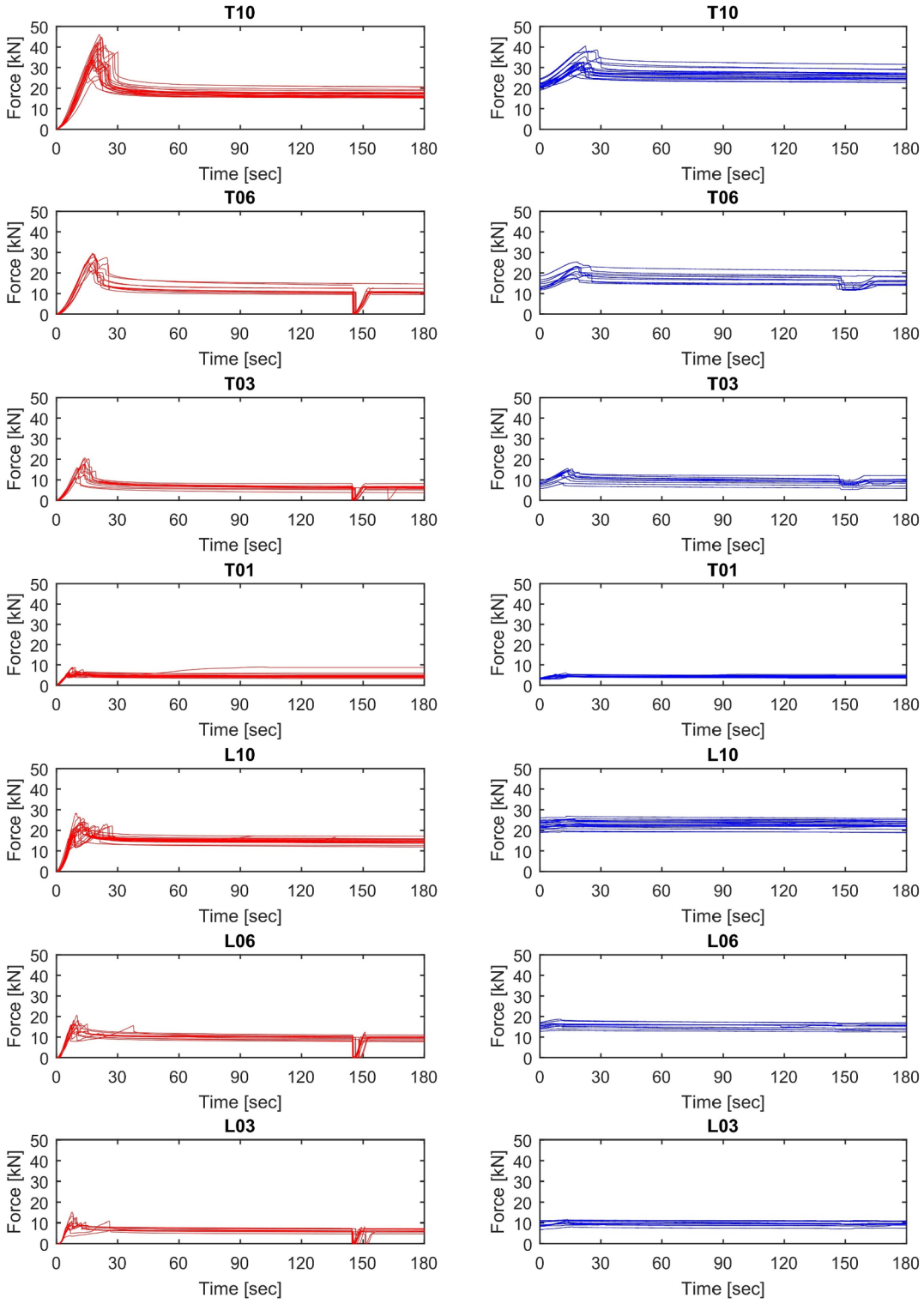

Fig. 6. Results of the friction experiments (left – red: force from the loading machine, right – blue: pre-stressing force). (For interpretation of the references to colour in this figure legend, the reader is referred to the web version of this article.)

by $\mu_{ki} = F_{10}/2P_{10}$, where F_{10} is the loading force applied from the machine when the displacement of loading application plate (Fig. 4b) is equal to 10 mm, and P_{10} is the corresponding pre-stressing force.

According to NS-EN 14358 [17], it is appropriate to consider the distribution of the friction coefficient as lognormal. Thus, in Table 3 the mean value of the measured friction coefficients, based on the lognormal distribution, is given. The friction coefficients for each specimen and the full derivation of their mean values are given in Appendix A.

Furthermore, the average vertical slip u_s for each series corresponding to the maximum static force F_s is given in Table 3.

From the plots in Fig. 6, it is evident that once the initial static phase is passed, the friction coefficient does not reach again the static value even if the test is stopped and restarted. Indeed, the plots in Fig. 6 show that after an unloading/reloading cycle the force returns approximately to the value acting before the unloading. Furthermore, it can be noted that the response of the specimens tested in the transversal direction

Table 3
Friction coefficients and vertical slips obtained from experiments.

Series	Static friction coefficient, μ_{st} [–]	Kinetic friction coefficient, μ_{ki} [–]	Vertical slips, u_s [mm]
T10	0.57	0.33	1.69
T06	0.62	0.34	1.56
T03	0.67	0.33	1.04
T01	0.67	0.52	0.81
*L*10	0.46	0.33	1.27
L06	0.51	0.32	1.06
L03	0.47	0.33	1.11

shows an initial non-linear rubber-like behavior, probably due to local effects of the cell wall structure of wood, which seems to be absent in the longitudinal series.

2.2.2. Numerical simulations

The numerical simulations of the friction experiments were performed with the parameters given in Chapter 2.1.2, and the average kinetic coefficient ($\mu_{ki} = 0.33$) as evaluated in Chapter 2.2.1. The kinetic coefficient of the series T01 is excluded in the computation of the average since it is much higher than the others. A comparison between experiments and numerical results from Abaqus is given in Fig. 7, where the dotted lines represent the experimental results and the continuous lines represent the results obtained from the simulations.

The plots present force vs. displacement curves, where the force is the loading force applied by the testing machine, and the displacement is the displacement of the loading plate, which can be considered equal to the displacement of the top surface of the timber block B (see Fig. 5).

As visible in Fig. 7, no attempt has been made to incorporate the effect of the static friction. From the plots, it is concluded that the use of the measured kinetic friction coefficient directly in numerical simulation will represent the effect of kinetic friction well at all stress levels, except for the lowest (0.1 MPa) where it is quite conservative.

3. Numerical simulations of SLT deck experiments

3.1. Material and methods

The full scale experiments on stress-laminated timber decks performed by Dahl [12,14] were used for comparison to numerical simulations presented herein. These decks were put together by timber of the European class C24. Each deck was made of 64 beams mounted side by side edgewise. The beam were all 5200 mm long and had cross-section of 48 × 222 mm^2 (see Fig. 8a). The experimental decks were pre-stressed by means of steel rods obtaining a stress-laminated (SLT) deck. The decks were continuously supported along the two shorter sides, with a distance between the supports of 5100 mm. The load was transferred by a 200 × 600 mm^2 steel plate located at the middle of the deck width. However, the steel plate was not located exactly in the mid-span due to technical issues. The distance between the axis of the plate and the supports was respectively 2480 mm (left) and 2620 mm (right), as shown in Fig. 8b.

Also the numerical simulations of the experimentally tested decks were performed in the FEM software program Abaqus. The geometry of the model resembles the geometry of the tested decks. The deck model consists of 64 beams, 5200 mm long and cross-section of 48 × 222 mm^2. The deck is vertically (y-direction; see Fig. 8b) supported on two lines lying parallel to the z-axis at 50 mm from the short edges of the deck. The support locations are displayed with dashed lines in Fig. 8b. The pre-stress is uniformly applied on the front surface (lying in the xy-plane; see Fig. 8a), while the nodes on the opposite surface (lying in the xy-plane) are prevented to displace in the z-direction. The contact interaction between the beams is defined as “hard” contact for the normal behavior and with a penalty formulation for the tangential behavior. The load is applied on a surface on the top of the deck (see Fig. 8) resembling the loading area of the experimental configurations.

The material properties used in the simulations of the decks are given in Table 4, where the x-direction is the longitudinal (see Fig. 8). The longitudinal modulus of elasticity E_x is chosen according to [12], the transversal moduli of elasticity $E_y = E_z$ are chosen according to [18], the shear moduli are chosen according to [19].

The three pre-stress levels listed in Table 5 were simulated, and each simulation is named after its pre-stress level.

3.2. Results and discussion

The simulations were performed by applying a normal compressive stress to the loading area (Fig. 8a) equivalent to a total force of 100 kN. The friction coefficient between the timber laminations was chosen according to the kinetic coefficient ($\mu_{ki} = 0.33$) evaluated in Chapter 2.2.1.

The results of the simulations are given in Fig. 9, where they are compared to the results of the full-scale experiments performed by Dahl, for a load of 100 kN [12]. In Fig. 9, the displacement shown in the y-axis refers to the displacement in the mid-span of the deck with respect to five different locations along the deck width W (visualized with a cross and Latin capital letters A to E in Fig. 8b). The unfilled circles are the measurements from the experiment, while the filled circles represent the results from the simulations. The lines in Fig. 9 are just linear interpolations between the data points and refer neither to measured nor to numerical displacement distribution.

The displacements in Fig. 9 show good agreement between experimental and numerical results, particularly for a pre-stress level of 0.6 and 1.0 MPa. However, the simulated decks are slightly stiffer than the experiments. This might be due to the different boundary conditions, since the vertical supports in the experimental deck did not prevent possible uplift at the supports, while in the simulations the supports prevented all movements in the vertical direction.

A summary of the results together with an evaluation of the Root Mean Square Deviation (RMSD) of the numerical displacements is provided in Table 6.

4. Alternative deck configurations

4.1. Butt joints configurations

4.1.1. Material and methods

In addition to the simulations of the deck experiments, more deck configurations were modelled. In these simulations, the influence of various butt joint distributions on the structural behavior of the deck was studied. The reference deck, denoted “Ref Plate” in Table 7, is an orthotropic plate having the same dimensions of the deck described in Chapter 3, and the elastic properties as given in Table 4. The deck tested by Dahl is described in Chapter 3 and is denoted “No B” since it does not contain butt joints. Additionally, two configurations with a different number of butt joints were simulated (B8 and B4). The configuration H4 differs from the B4 only for the height of the deck beams. The configurations are summarized in Table 7.

All the configurations were tested under the effect of Load Model 1 and Load Model 2, as defined in Eurocode 1 [20], using the characteristic combination of actions as defined in Eurocode 0 [21]. The characteristic (or rare) combination is used for irreversible serviceability limit states when investigating permanent unacceptable deformation or local damage.

Load Model 1 and 2 are displayed in Fig. 10. Load Model 1 consists of a double-axle concentrated load (tandem system; TS1 and TS2) and a uniform distributed load (UDL). The UDL is set equal to 5.4 kN/m^2 in the lane that gives the most unfavorable effects (Lane 1), and equal to 2.5 kN/m^2 in the rest of deck (in the unfavorable parts of the influence surface). Each axle of the tandem system represents two wheels (contact surface: 0.4 × 0.4 m^2). The concentrated load is set equal to 150 kN for each wheel in the Lane 1, 100 kN in the Lane 2, 50 kN in the Lane 3

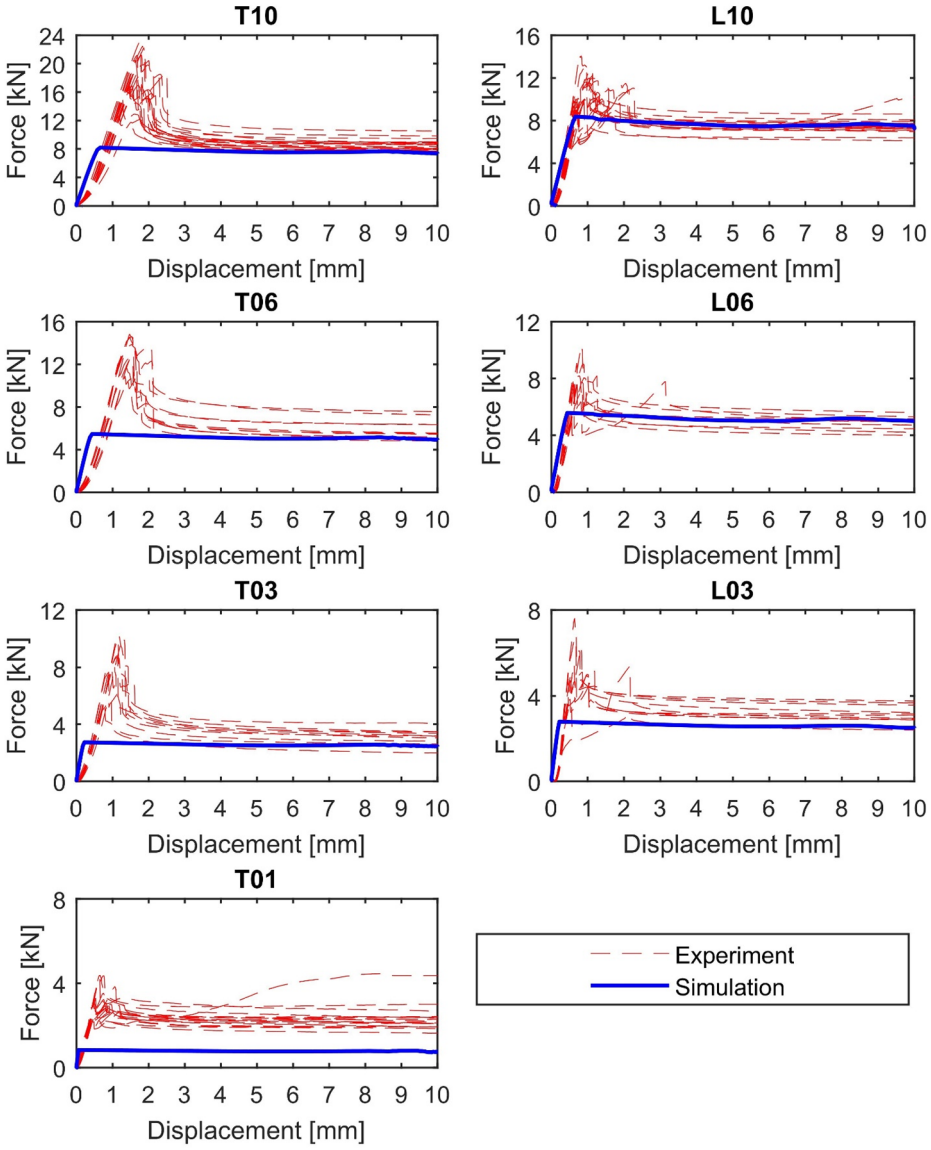

Fig. 7. Comparison between experimental results and numerical simulations of the friction tests (left: transversal; right: longitudinal).

where the lanes are numbered in decreasing order starting from the one that gives the most unfavorable effects. In all other possible lanes, the tandem system is not present [20].

The simulated decks with widths of 3072 mm consist only of a single lane (Lane 1). Load Model 2 consists of a single-axle concentrated load (CL) and the contact surface of the two wheels of the axle is rectangular (0.60×0.35 m^2). The concentrated load for Load Model 2 is set equal to 200 kN for each wheel.

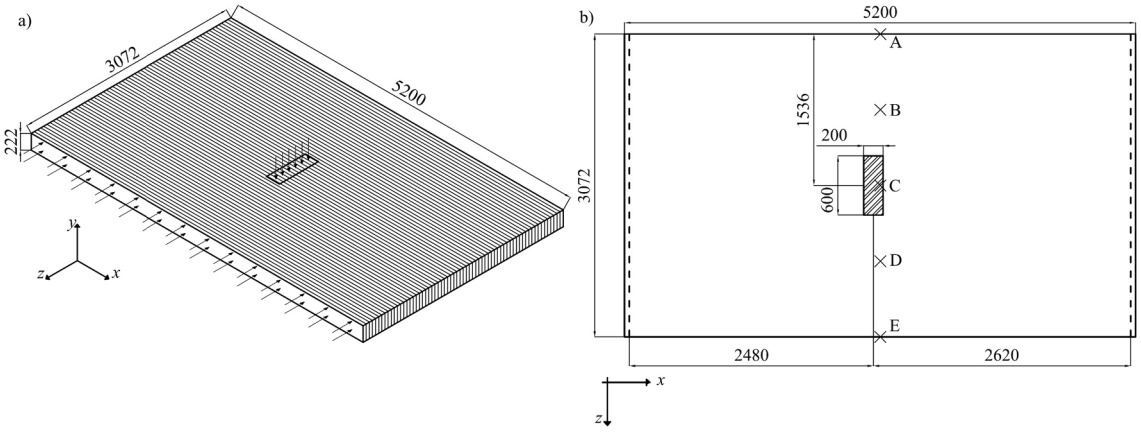

Fig. 8. Geometry of the deck: a) Isometric view; b) plane view (dashed lines indicate simply supports).

Table 4
Elastic properties of wood used in deck simulations.

Normal moduli	[MPa]	Shear moduli	[MPa]	Poisson's ratios	[–]
E_x [(a)]	12,000	$G_{xy} = G_{xz}$ [(c)]	600	$\nu_{xy} = \nu_{xz} = \nu_{yz}$	0
$E_y = E_z$ [(b)]	240	G_{yz} [(c)]	31		

[(a)] from [12], [(b)] from [18], [(c)] from [19].

Table 5
Summary of the performed simulations.

Name	Pre-stress [MPa]
D100	1.0
D60	0.6
D10	0.1

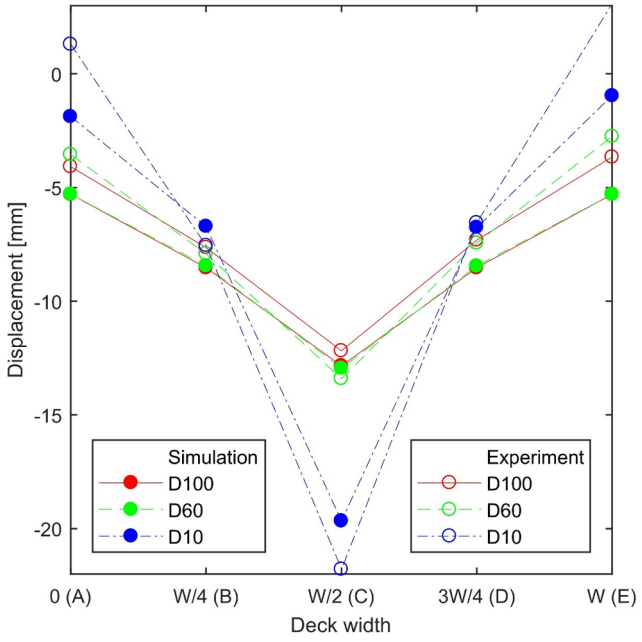

Fig. 9. Comparison between full-scale deck experiments and simulations.

4.1.2. Results and discussion

Table 8 gives the results of the numerical simulations of the evaluated deck configurations described in Chapter 4. Table 8 shows the maximum longitudinal stress, shear stress, vertical displacement and longitudinal curvature of each deck configuration with respect to the values of the reference plate. In addition, the maximum interlaminar slip for each simulated deck configuration is given. In Table 9, the flexural stiffness of the deck configurations with respect to the reference plate is compared with the NPRA recommended reduction ratio [8] and with the factors suggested by Ritter [5] and by Crews [9]. The maximum longitudinal stress, the maximum vertical displacement and longitudinal curvature were evaluated under the effect of Load Model 1, while the maximum shear stress and the maximum slip between the timber beams were evaluated under the effect of Load Model 2.

From the results shown in Table 8, it is clear that the flexural stiffness in the deck is reduced due to presence of the butt joints. The Norwegian Public Roads Administration (NPRA) [8] suggests reducing the flexural stiffness by the factor $\frac{n}{1+n}$, where n is the number of beams per butt joint in a transversal cross-section of the SLT deck. Ritter's factor is taken from its guidelines [5] based on the butt joint frequency. Crews' factor can be approximated as $\frac{n-1}{n}$, where n has the same meaning as in the NPRA ratio [9].

Both Crews' factor and the NPRA ratio overestimate the stiffness reduction in the configurations B4 and B8, while Ritter's factor underestimates it for the configuration B8 (Table 9). However, the difference between the simulation values and the NPRA recommendations is only about 2%, and is deemed to be a good estimate of the stiffness reduction. As the flexural stiffness decreases, the vertical displacement and the longitudinal curvature increases with the amount of butt joints. However, the longitudinal surface strains remained limited ($< 2‰$) in all the tested configurations.

The maximum interlaminar slip was found to be of the order of 2 mm in the deck configurations No B, B8, B4 and H4 (Table 8). This is more than the slip measured in the friction tests, shown in Table 3, and thus the choice of using the kinetic values as friction coefficient seems reasonable.

4.2. Pre-stress patterns

4.2.1. Material and methods

In the simulations of the configurations in Table 7, a pre-stress of 1 MPa was applied uniformly on the outer beams. However, the effect of different types of pre-stressing system was also evaluated. In addition to the ideal uniform compressive stress applied over the whole exterior beams, several alternative distinct plate patterns for application of compressive stresses were simulated on configurations without butt joints. These plate patterns are shown in Fig. 11.

In all patterns, the pre-stress is applied on square plates with dimension of 200 mm. Twelve different geometries were simulated with varying deck height and spacing between the areas of application of the pre-stress. The simulations are named after the plate pattern, followed by an indication of the spacing of the pre-stressing area S and the deck height H; confer Fig. 11 and Table 10. The objective of these simulations is to study the stress distribution in both the transversal and longitudinal directions.

4.2.2. Results and discussion

In all configurations, the pre-stress tends to become uniform with the increase of the distance from the edge. In Table 11, it is given the transversal diffusion length l_t, i.e. the distance from the deck edge for which a uniform pre-stress (equal to 100 ± 1% of the pre-stress applied) occurs in the deck, and the longitudinal diffusion length l_l, i.e. the distance from the pre-stress application area for which a uniform pre-stress (100 ± 1%) occurs in the horizontal deck cross-section (see Fig. 12).

Table 6
Numerical displacements vs. experimental displacements and RMSD of the numerical results of the deck model.

Config.	Pre-stress [MPa]	Displacements [mm]										RMSD[mm]
		Width = 0		Width = W/4		Width = W/2		Width = 3 W/4		Width = W		
		Num	Exp	Num	Exp	Num	Exp	Num	Exp	Num	Exp	
D100	1.0	−4.08	−5.30	−7.64	−8.53	−12.18	−12.84	−7.31	−8.53	−3.66	−5.29	1.17
D60	0.6	−3.55	−5.30	−7.92	−8.44	−13.40	−12.95	−7.44	−8.45	−2.75	−5.30	1.48
D10	0.1	1.30	−1.88	−7.55	−6.71	−21.79	−19.66	−6.55	−6.75	3.08	−0.96	2.51

Table 7
Simulated deck configurations for butt joint evaluation.

Name	Span length [m]	Height beams [mm]	Number of butt-joints	Distance between butt-joints [m]
Ref Plate	10.8	222	0	–
No B	10.8	222	0	–
B8	10.8	222	1 every 8 beams	1.2
B4	10.8	222	1 every 4 beams	1.2
H4	10.8	450	1 every 4 beams	1.2

The plots with the distribution of the pre-stress obtained for all the simulated configurations are given in Appendix B. Moreover, the transversal and the longitudinal diffusion angle, θ_t and θ_l respectively, are given in Table 11 for each configuration.

It is evident that the aligned one-row arrangement (P1) is the least advantageous for distributing the stresses on the whole vertical deck cross-section, since the uniformity of the pre-stress is obtained at bigger distances than the other arrangements. The alternating pattern (P2) improves the distribution, while the fastest distribution of stresses is obtained with the two-row arrangement (P3). However, the P3 pattern requires for the same spacing a double amount of pre-stressing rods. A comparison of effectiveness of pattern systems should also take the number of pre-stressing rods per unit length of the bridge into account.

Moreover, the diffusion angles obtained from the simulations are lower than the Eurocode suggested values, which suggests a 15° diffusion in the transversal direction and a 45° diffusion in the longitudinal direction [7].

The transversal diffusion angles θ_t change fairly linearly with the vertical distance x between the plate edge and the deck edge (see Fig. 11). An approximation for its evaluation can be written as Eq. (1), where θ_t is expressed in degrees and x is expressed in mm.

$$\begin{aligned} &\text{P1: } \theta_t = 6.5 + 0.0066x \\ &\text{P2: } \theta_t = 1.35 + 0.02x \\ &\text{P3: } \theta_t = 1.9 + 0.02x \end{aligned} \quad (1)$$

4.3. Transverse tensile stress

4.3.1. Material and methods

In order to explore if the pre-stress generated by the alternative patterns is sufficient to avoid gaps between the laminations, and if any pattern of pre-stressing is superior to others, a study was performed using the transverse tensile stress generated by the applied loads on the deck as the primary parameter of interest. In these simulations, the deck was modelled as an orthotropic plate, similarly to the deck denoted "Ref Plate" described in Chapter 4.1.1, and the elastic properties as given in Table 4. No pre-stress was applied on the plate. The applied load taken into consideration was the Load Model 2 from Eurocode 1, as it is the most critical for the evaluation of the transverse behavior of orthotropic decks [21]. The layouts of the decks tested for the transverse tensile stress study are given in Table 12. The deck width was equal to 3000 mm in all the layouts and it is vertically supported on the bottom edge parallel to the z-axis, with distance between the supports equal to *DS* (Fig. 13).

4.3.2. Results and discussion

Since the pre-stress becomes uniform after the diffusion length l_t from the deck edge, the transverse tensile stress must be limited in proximity of the edge in order to avoid gaps between the laminations.

In Fig. 14, the transverse stresses obtained from the numerical simulations listed in Table 12 are given. All plots refer to the transversal cross-section with the highest tensile stresses obtained from the simulations (i.e. deck bottom edge). The stresses are positive in proximity of the edge, reaching the peak about 650 mm distant from the deck edge and turning into compressive stresses about 1100 mm from the deck edge. However, after circa 2500 mm from the edge, the stresses again become positive, especially for decks with heights less than 500 mm. Among layouts with the same deck height, the layouts that reach the highest tension stress, and maintain it for a longer distance, are the layouts with 350 mm distance between supports. The support distance can resemble the spacing of transverse supporting beams in a bridge. The results in Fig. 14 show that when the distance between the supports increases (large distances are more common in real decks), the tensile stresses tend to decrease. Moreover, increasing height of the decks gives decreasing tensile stresses.

In Table 13, it is given the peak stress σ_{max} for all the layouts with support spacing equal to 350 mm. Note that the layouts shown in Table 13 are the ones giving the largest tensile stresses.

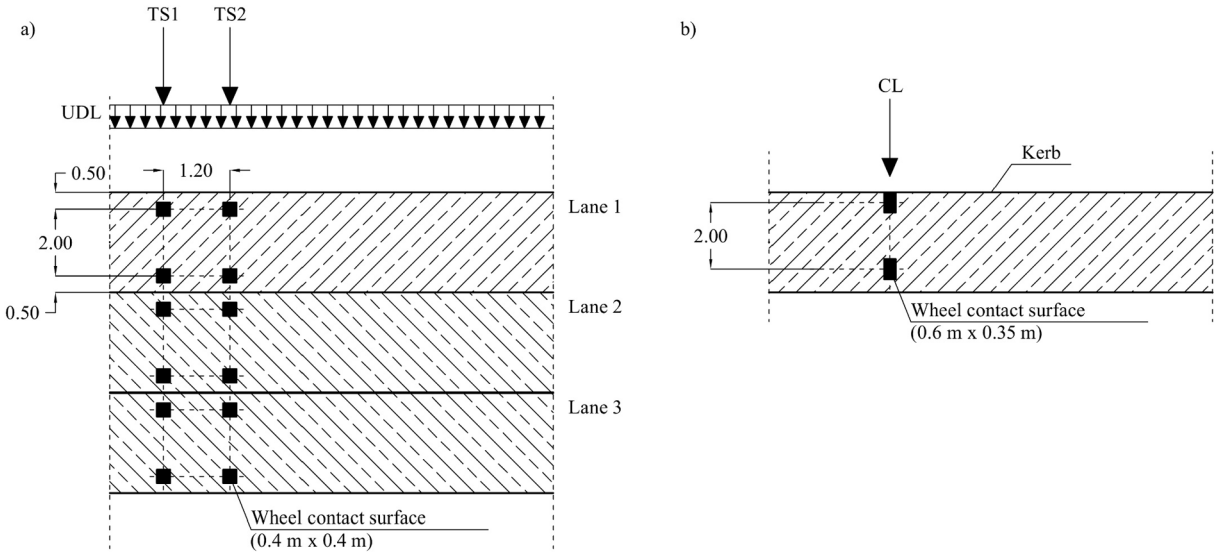

Fig. 10. a) Load Model 1; b) Load Model 2 (units in m).

Table 8
Summary of the results of the numerical simulations.

Name	Max longitudinal stress ratio[a]	Max shear stress ratio[b]	Max vertical displacement ratio[a]	Max longitudinal curvature ratio[a]	Max interlaminar slip[b] [mm]
Ref Plate	1	1	1	1	–
No B	1.056	0.985	1.061	2.3	2.2
B8	1.102	0.914	1.095	6.7	2.2
B4	1.226	0.874	1.137	9.6	2.5
H4	0.273	0.525	0.207	0.3	2.5

The ratios are calculated with respect to the Ref Plate values.
[a] Under Load Model 1.
[b] Under Load Model 2.

Table 9
Comparison of the flexural stiffness ratio from simulations with recommendations from literature.

Name	Flexural stiffness ratio*	NPRA ratio: $\frac{n}{1+n}$	Crews' factor	Ritter's factor
Ref Plate	1	1	1	1
No B	0.947	1	1	1
B8	0.907	0.889	0.875	0.930
B4	0.816	0.800	0.750	0.800

* The values are ratios with respect to the Ref Plate values.

4.3.3. Design recommendations

The development of the pre-stress for the most critical section in proximity of the edge deck for the different simulated deck patterns (P1, P2 and P3) is presented in Fig. 15. In all the simulations, a uniform pre-stress (100 ± 1% in the plots) is reached after some diffusion length. In each plot, there are four curves corresponding to a different spacing, *S* in Fig. 11 (from left to right: 300 mm, 500 mm, 700 mm and 1000 mm). However, some of the curves overlap each other.

For decks 750 mm or 1000 mm high, the *one-row* pattern P1 does not manage to develop enough pre-stress within 650 mm, and therefore it is not recommended for such high decks. In addition to a sufficient pre-stressing force, it is suggested to limit the spacing to 750 mm for decks 750 mm high and to 500 mm for decks 1000 mm high, when using the *alternating* pattern P2 order to develop sufficient pre-stress within 650 mm. On the other hand, the *two-row* pattern P3 can be used for tall decks providing a sufficient pre-stressing force. For decks up to 500 mm high, all the patterns are suitable. The required pre-stress values necessary to avoid completely tensile stresses in any location of the deck are given in Table 14.

Note that the values in Table 14 are quite conservative, since they are evaluated comparing the pre-stress in the most critical section for its development (i.e. the furthest from the pre-stressing plates), to the transverse

Table 10
Simulations for pre-stressing pattern evaluation.

Name	Spacing pre-stress *S* [mm]	Deck height *H* [mm]
PX-300-500	300	500
PX-500-500	500	500
PX-750-500	750	500
PX-1000-500	1000	500
PX-300-750	300	750
PX-500-750	500	750
PX-750-750	750	750
PX-1000-750	1000	750
PX-300-1000	300	1000
PX-500-1000	500	1000
PX-750-1000	750	1000
PX-1000-1000	1000	1000

X represents the pre-stress pattern and it is equal to 1, 2 or 3 as visualized in Fig. 11.

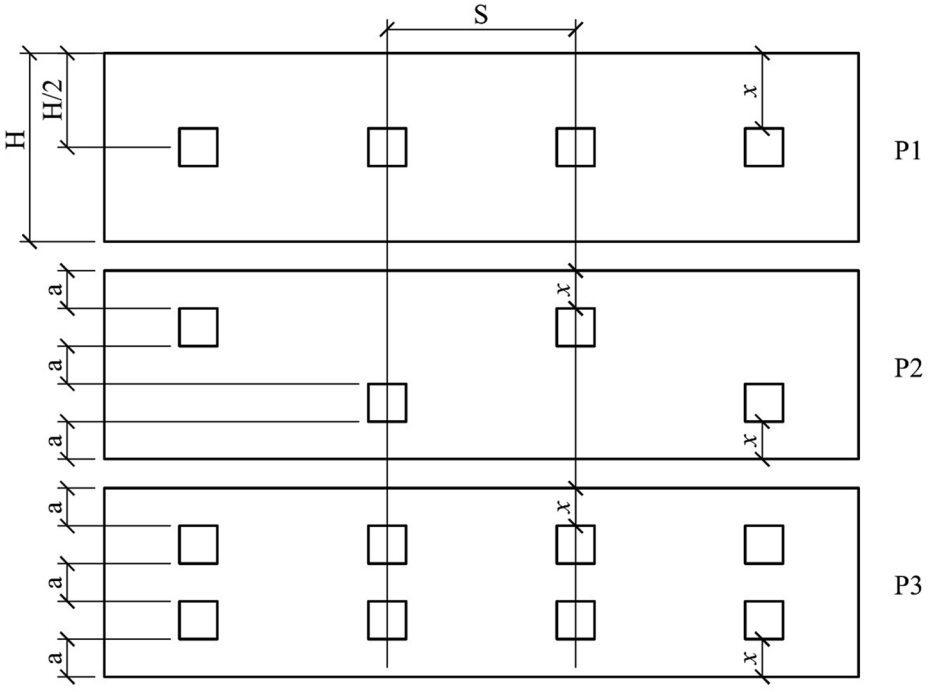

Fig. 11. Alternative simulated pre-stress plate patterns (top: P1, middle: P2, bottom: P3).

Table 11
Transversal and longitudinal diffusion length and respective diffusion angles.

Config.		S = 300 mm			S = 500 mm			S = 750 mm			S = 1000 mm		
	H[mm]	500	750	1000	500	750	1000	500	750	1000	500	750	1000
P1	l_t[mm]	1150	1850	2500	1150	1850	2500	1150	1850	2500	1150	1850	2500
	θ_t[°]	7.4	8.5	9.1	7.4	8.5	9.1	7.4	8.5	9.1	7.4	8.5	9.1
	l_l[mm]	250	250	250	300	300	300	500	500	500	700	700	700
	θ_l[°]	11.3	11.3	11.3	26.6	26.6	26.6	28.8	28.8	28.8	29.7	29.7	29.7
P2	l_t[mm]	950	1700	2150	950	1700	2150	950	1700	2150	950	1700	2150
	θ_t[°]	2.0	3.9	5.3	2.0	3.9	5.3	2.0	3.9	5.3	2.0	3.9	5.3
	l_l[mm]	350	350	350	700	700	700	800	800	800	950	950	950
	θ_l[°]	29.7	29.7	29.7	29.7	29.7	29.7	39.1	39.1	39.1	43.5	43.5	43.5
P3	l_t[mm]	800	1450	2050	800	1450	2050	800	1450	2050	800	1450	2050
	θ_t[°]	2.4	4.6	5.6	2.4	4.6	5.6	2.4	4.6	5.6	2.4	4.6	5.6
	l_l[mm]	250	250	250	300	300	300	500	500	500	700	700	700
	θ_l[°]	11.3	11.3	11.3	26.6	26.6	26.6	28.8	28.8	28.8	29.7	29.7	29.7

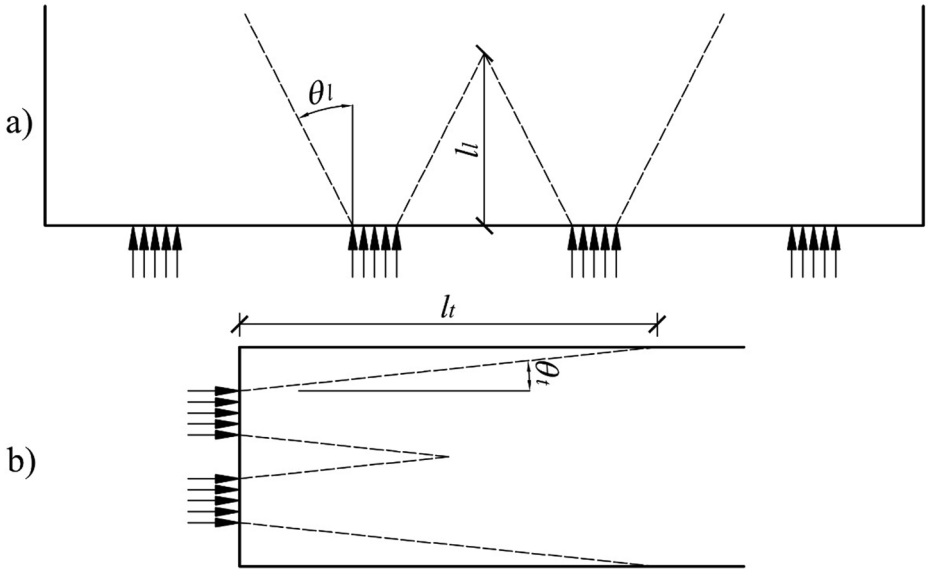

Fig. 12. Diffusion lengths and angles. a) Horizontal deck cross-section; b) Vertical transversal deck cross-section.

Table 12
Simulated layout for transverse tension study.

Name	Deck height *H* [mm]	Distance between supports *DS* [mm]
DS-1000-250	1000	250
DS-1000-350	1000	350
DS-1000-500	1000	500
DS-1000-1000	1000	1000
DS-1000-3000	1000	3000
DS-500-250	500	250
DS-500-350	500	350
DS-500-500	500	500
DS-500-1000	500	1000
DS-500-3000	500	3000
DS-750-350	750	350
DS-250-350	250	350

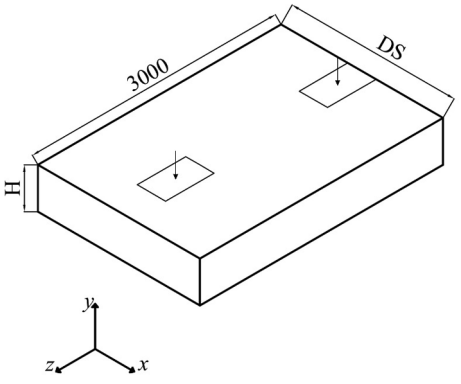

Fig. 13. Geometry of the decks tested for the transverse tensile stress study (unit in mm).

tensile stresses in the cross-section where the tension is highest (i.e. deck bottom edge). Moreover, increasing the distance between the supports (e.g. transverse beams) results in decreasing tensile stresses (Fig. 14), and thus the recommendations of Table 14 may be lowered.

Fig. 14 shows that there are typically two domains which might lead to tensile stresses: one in proximity of the edge with distance to edge less than 1 m, and the other from about 2.5 m from the edge. Hence, it is recommended to achieve a uniform pre-stress over the vertical cross-section less than 2500 mm from the edge. The results in Table 11 show that this is possible for all the simulated configurations since the uniformity of the stresses occurs at distances less than 2500 mm from the edge. Moreover, at 1900 mm from the edge, any point in the deck cross-section is subjected to a pre-stress at least equal to 95% of the uniform expected value for any layout, since the stress diffusion is not linear through the deck width. Therefore, if the uniform pre-stress value is sufficient to cover the maximum stress from the loads, then the tensile stresses are overcome.

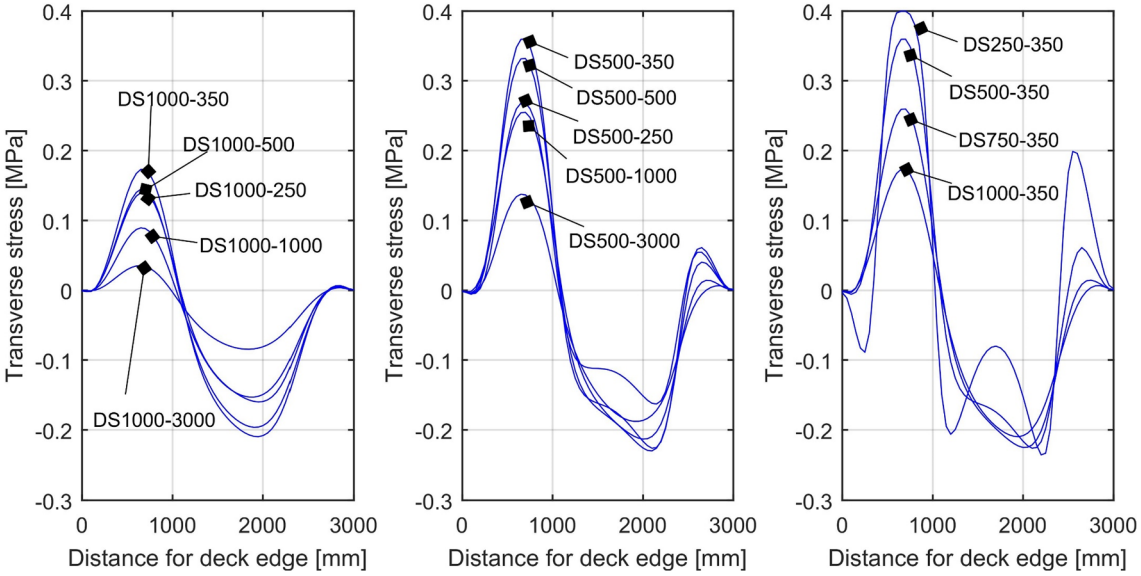

Fig. 14. Transverse stresses for the simulated layouts (left: deck height = 1000 mm; center: deck height = 500 mm; right: supports distance = 350 mm).

Table 13
Peak tensile stress for the layouts S-H-350.

Layout	σ_{max} [MPa]
DS-250-350	0.40
DS-500-350	0.36
DS-750-350	0.26
DS-1000-350	0.17

The recommendation of uniformity of the pre-stress at 2500 mm from the edge provides guidelines for the spacing of the pre-stress areas. Indeed, the spacing has to be small enough so that the longitudinal diffusion manages to make the pre-stress uniform in any horizontal deck cross-section. Table 11 showed that the longitudinal diffusion angle tend to increase if the spacing increase. It is thus on the safe side to use the maximum longitudinal diffusion angle obtained from the simulations, $\theta_l \cong 30^\circ$ for the configurations P1 and P3 and $\theta_l \cong 45^\circ$ for

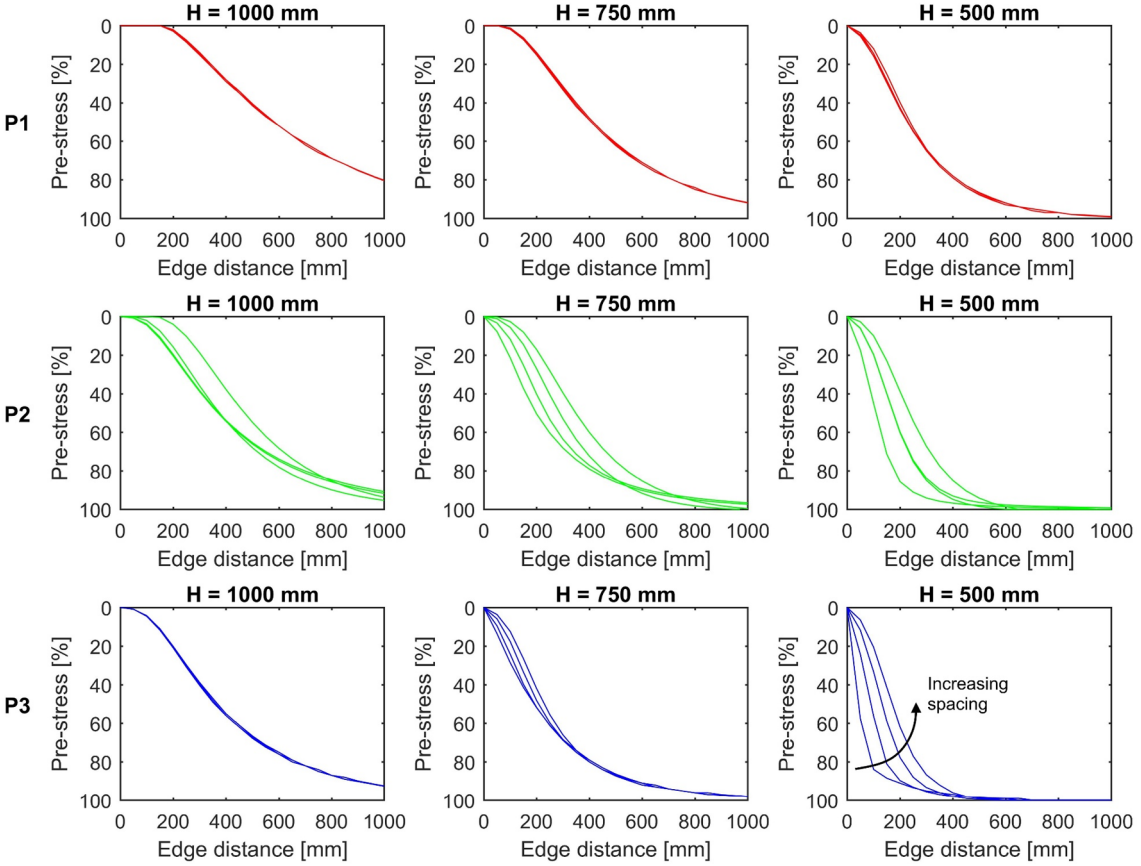

Fig. 15. Pre-stress development in proximity of the edge for the most critical section (some of curves overlap but however each plot contains 4 different curves corresponding to a different spacing: from left to right 300 mm, 500 mm, 750 mm and 1000 mm).

Table 14
Minimum pre-stress required to avoid gaps [MPa].

Configuration	Spacing [mm]	Height [mm]		
		500	750	1000
P1	300	0.83	–	–
	500	0.83	–	–
	750	0.83	–	–
	1000	0.83	–	–
P2	300	0.80	0.61	0.50
	500	0.80	0.61	0.50
	750	0.80	0.62	0.50
	1000	0.80	0.63	–
P3	300	0.78	0.60	0.48
	500	0.78	0.60	0.48
	750	0.78	0.60	0.48
	1000	0.79	0.61	0.48

the configuration P2, for the evaluation of the maximum allowed spacing. Hence, the maximum allowed spacing for the configuration P1 and P3 results in circa 3000 mm, while for the configuration P2 circa 2500 mm. Note that the configuration P3 requires twice as many pre-stressing rods with the same spacing, and thus in this sense, the configuration P2 is the most effective.

However, a large spacing in a SLT deck results in high compression stress orthogonal to grain on the exterior beams. Therefore, the compression under the pre-stressing plates might be the most restrictive factor for the choice of spacing between the pre-stressing bars.

5. Conclusion

The objective of this study was to explore some design issues of pre-stressed timber bridge decks regarding the effects of friction between lamellas, butt joints and pre-stressing rods locations.

The experimental friction tests showed that the kinetic friction coefficient is similar for all the performed test series. The numerical simulations represent the results of the friction tests well by employing the kinetic friction coefficient of 0.33. Furthermore, the friction model, together with representative material modeling in numerical FEM models, shows good agreement with full-scale deck test measurements. Thus, the friction coefficient in numerical analyses can be taken equal to 0.33 for softwood lamellas in pre-stressed timber decks.

The same numerical model approach was used to study the effect of butt joints on the stiffness of stress-laminated timber decks, as well as the influence of pre-stressing rods distribution on the transversal compression.

The results from the simulations show that the presence of butt joints reduces the overall flexural stiffness of the deck and the recommendation from NPRA are deemed to be sufficient for design purposes.

The interlaminar slip in the simulated decks exceeds the average slip measured in the experiment at the start of the kinetic phase. The experiments showed that after the initial static phase was passed the static friction coefficient was not anymore achievable. Hence, the choice of the kinetic value as friction coefficient is probably most suitable for SLT deck simulations.

Finally, three different pre-stress configurations were studied. All the configurations guarantee a uniform transversal compression stress in the deck after some distance from the edge (diffusion length). However, the alternating pattern (P2) diffuses the pre-stress faster than the one-row linear pattern (P1). The fastest diffusion occurs using the two-row pattern (P3), which however requires twice as many rods per meter if the spacing is the same. Moreover, the pattern P1 should not be used in deck higher than 500 mm since it does not manage to develop enough pre-stress in proximity of the deck edge to overcome the transversal tensile stress due to the traffic load on the deck. Both the pattern P2 and P3 might be used for decks up to 1000 mm, respecting the requirements on pre-stress level and spacing given in Table 14. However, the pattern P2 may be preferable for decks between 500 and 750 mm high, since it contains half of the pre-stressing rods compared to the pattern P3. Eventually, the longitudinal pre-stress diffusion would allow large spacing, but the limitations given by the compression orthogonal to grain on the exterior deck beams must be considered.

CRediT authorship contribution statement

Francesco Mirko Massaro: Conceptualization, Methodology, Software, Validation, Formal analysis, Investigation, Writing - original draft, Writing - review & editing, Visualization. **Kjell Arne Malo:** Writing - review & editing, Supervision.

Declaration of Competing Interest

The authors declare that they have no known competing financial interests or personal relationships that could have appeared to influence the work reported in this paper.

Acknowledgments

This work was mainly funded by the WoodWisdom-Net+ project DuraTB (“Durable Timber Bridges”). The friction tests were additionally funded by the Norwegian Public Roads Authority (NPRA). The supports from the funding bodies and partners are gratefully acknowledged. The authors would also like to acknowledge Anette Karlsen Paulsrud, Andreas Gladbakke and Lars Henning Krokengen for their contribution in the experimental work.

Appendix A. Supplementary material

Supplementary data to this article can be found online at https://doi.org/10.1016/j.engstruct.2020.110592.

References

[1] Bell K. Timber bridges. In: Augustin M, editor. Handbook 1 - Timber Structures: Leonardo da Vinci Pilot Project, Educational Materials for Designing and Testing of Timber Structures - TEMTIS; 2008. p. 211–26.
[2] Malo KA. Timber bridges. In: Pipinato A, editor. Innovative bridge design handbook. Boston: Butterworth-Heinemann; 2016. p. 273–97.
[3] Crocetti R. Timber bridges: General issues, with particular emphasis on Swedish typologies. 20 Internationales Holzbau-Forum IHF. Garmisch-Partenkirchen, Germany; 2014. p. 359–70.
[4] Massaro FM, Malo KA. Anchor plates for pre-stressing rods and compression orthogonal to grain of timber. In: 3rd International Conference on Timber Bridges - ICTB 2017. Skellefteå, Sweden; 2017. p. 42–51.
[5] Ritter MA. Timber bridges: design, construction, inspection, and maintenance. Washington DC: U.S. Department of Agriculture, Forest Service; 1992.
[6] Ekholm K. Performance of Stress-Laminated Timber Bridge Decks [Doctoral dissertation]. Gothenburg, Sweden: Chalmers University of Technology; 2013.
[7] CEN. Eurocode 5: Design of timber structures – Part 2: Bridges. EN 1995-2:2004: Comité Européen de Normalisation; 2004.
[8] Statens vegvesen. Håndbok N400 Bruprosjektering - Prosjektering av bruer, ferjekaier og andre bærende konstruksjoner: Vegdirektoratet; 2015.
[9] Crews KI. Behaviour and critical limit states of transversely laminated timber cellular bridge decks [Doctoral dissertation]. Sydney: University of Technology; 2002.
[10] Ekholm K, Kliger R. Effect of vertical interlaminar shear slip and butt joints in narrow stress-laminated-timber bridge decks. Eng Struct 2014;72:161–70.
[11] Kalbitzer T. Stress-laminated Timber Bridge Decks: Experiments regarding the Coefficient of Friction between Laminations [Master thesis]. München: Technische Universität München; 1999.
[12] Dahl KB, Bovim NI, Malo KA. Evaluation of stress laminated bridge decks based on full scale tests. In: 9th World Conference on Timber Engineering. Portland, OR, USA; 2006.
[13] Dassault Systemes. Abaqus/CAE 6.14. 2014.
[14] Dahl KB. Tverrspente dekker i tre - Vurdering av aktuelle beregningsmetoder basert på fullskala forsøk (eng.: Stress laminated wood decks - Evaluation of current design procedures based on full scale testing) [Master thesis]. Ås: NLH - Norwegian College of Agriculture; 2002.
[15] CEN. Timber structures - Glued laminated timber and glued solid timber. EN 14080:2013: Comité Européen de Normalisation; 2013.

[16] Koubek R, Dedicova K. Friction of wood on steel [Master thesis]. Växjö: Linnaeus University; 2014.
[17] CEN. Timber structures - Calculation and verification of characteristic values. EN 14358:2016: Comité Européen de Normalisation; 2016.
[18] Massaro FM, Malo KA. Long-term behaviour of norway spruce glulam loaded perpendicular to grain. Eur. J. Wood Wood Prod. 2019.
[19] Dahl KB. Mechanical properties of clear wood from Norway spruce [Doctoral dissertation]. Trondheim: Norwegian University of Science and Technology; 2009.
[20] CEN. Eurocode 1: Actions on structures – Part 2: Traffic loads on bridges. EN 1991-2:2003: Comité Européen de Normalisation; 2003.
[21] CEN. Eurocode 0: Basis of structural design. EN 1990:2002: Comité Européen de Normalisation; 2002.